Ego-noise Prediction Based on Multimodal Learning for Enhanced Discrimination in UAV Hammering Inspection

Koki Shoda[1], Jun Younes Louhi Kasahara[1], Hajime Asama[1], Qi An[2] and Atsushi Yamashita[2]

***Abstract*— In this paper, we propose an ego-noise prediction method applicable to Unmanned Aerial Vehicles (UAVs). Sensing sound using UAV has a significantly reduced Signal-to-Noise Ratio due to the strong ego-noise from the propellers and motors. Template-based ego-noise prediction for robots with pre-set movements, such as humanoid robots, has previously been studied. However, that approach is not applicable to UAVs which continuously adjust the propeller's rotation speed based on the situational requirements. Here, we propose a novel framework for ego-noise prediction by focusing on propellers, which are the main ego-noise source, and translating the modality of propeller vibrations into the modality of ego-noise sound. Assuming a strong relation between the vibration frequency of a propeller and the ego-noise it generates, we propose using a Recurrent Neural Network to predict the ego-noise spectrogram, using vibration frequency as a feature. The prediction accuracy of ego-noise spectrograms was at a level that suggests the potential for effective ego-noise reduction, and the results are promising for applications in UAV hammering inspection.**

I. INTRODUCTION

In recent years, many concrete social infrastructures have been aging, and their inspection has become an important issue [1]. The hammering inspection, consisting of hitting the surface and using the impact sound for inspection, has the advantages of being economical, simple, and non-destructive for internal detection of defects. Automation of hammering will reduce inspection costs and enable early defects detection [2]. Unmanned Aerial Vehicles (UAVs) are expected to be used as a means of automation, because they can shorten inspection time and enable inspections of difficult-to-access locations such as bridges [3]. However, sensing sound of hammering using UAV has a significantly reduced Signal-to-Noise Ratio (SNR) due to the strong ego-noise from the propellers and motors [4], interfering with discrimination of healthy or defective sounds [5].

Nishimura et al. [5] developed a hammering inspection system with a robot that runs stably with wheels on walls by thrust power from propellers. In that study, a Deep Neural Network (DNN) was trained to discriminate between healthy and defective sounds by inputting hammering sounds contaminated with steady ego-noise. However, such noise countermeasures do not work for typical UAVs because of the unsteady ego-noise generated by movement and attitude stabilization of UAVs. A robot that runs with wheels on walls can only move on flat surfaces and cannot inspect all parts of complex structures such as bridges. Therefore, the UAVs with fewer constraints on inspection locations are expected to be deployed for such tasks.

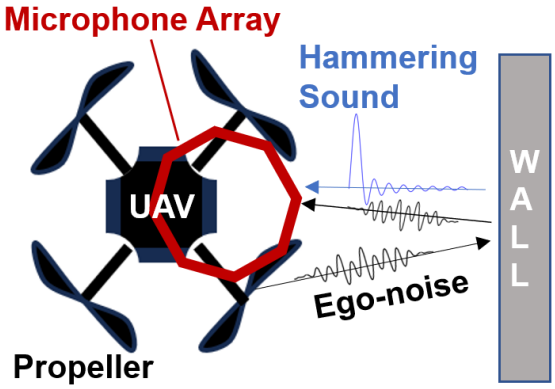

Fig. 1. Hammering sound and reverberating ego-noise coming from the same direction.

Another approach to enhance discrimination between healthy and defective sounds is ego-noise reduction during hammering inspection. In the single-channel microphone ego-noise reduction approach, Mukhutdinov et al. [6] trained a DNN to obtain clean speech by inputting noisy speech. However, when using UAVs for hammering inspection, ego-noise reverberation and environmental noise are different for each inspection location. Therefore, frequent retraining is expected to be necessary. Obtaining a large number of hammering sounds for retraining at each inspection point would exceedingly prolong the inspection time.

In the microphone array ego-noise reduction approach, Wang et al. [7] reduced ego-noise by directing space-filtering in the direction of a localized target sound source. Ego-noise reverberates against the wall and enters the microphone in the same way as hammering sound, as shown in Fig. 1. Since the UAV inspects against a surface, reverberating ego-noise reduction by space-filtering is not possible.

In the study of ego-noise reduction by predicted ego-noise subtraction, Ince et al. [8] pre-created a template database of ego-noise and predicted ego-noise from motor states using nearest neighbor search. However, this approach is specifically effective for robots with pre-set motion patterns, such as humanoid robots, and is not applicable to UAVs due to their dynamic nature, where the propeller's rotation speed is

[1]K. Shoda, J. Y. Louhi Kasahara and H. Asama are with the Department of Precision Engineering, Graduate School of Engineering, The University of Tokyo, 5-1-5 Kashiwanoha, Kashiwa, Chiba 277-8563, Japan {shoda, louhi, asama}@robot.t.u-tokyo.ac.jp

[2]Q. An and A. Yamashita are with Department of Human and Engineered Environmental Studies, Graduate School of Frontier Sciences, The University of Tokyo, 5-1-5 Kashiwanoha, Kashiwa, Chiba 277-8563, Japan {an, yamashita}@robot.t.u-tokyo.ac.jp

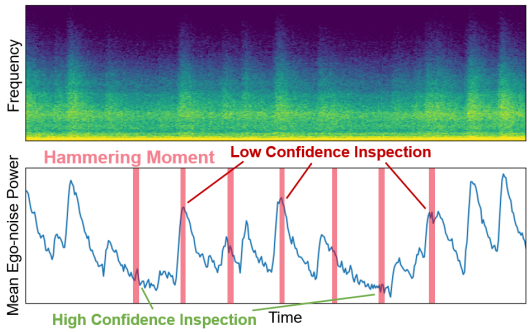

Fig. 2. Ego-noise spectrogram and its average power. The pink vertical bands represent the moments of hammering.

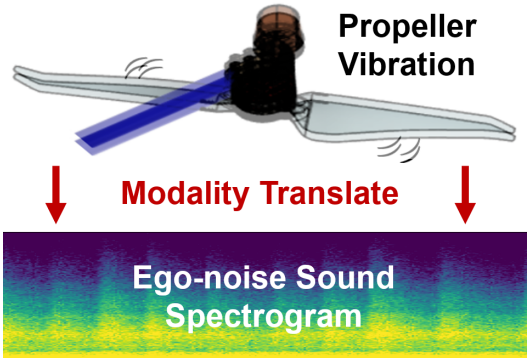

Fig. 3. Concept of proposed ego-noise prediction. Ego-noise prediction is performed by translating the modality of propeller vibrations into the modality of ego-noise sound.

continuously adjusted based on the situational requirements.

The objective of this study is to predict the diverse and unsteady ego-noise of UAVs. Here, we propose an ego-noise prediction framework applicable to UAVs by focusing on propellers as the main ego-noise source and translating the modality of propeller vibrations into the modality of ego-noise sound.

II. PROPOSED METHOD

A. Concept

If accurate ego-noise prediction during hammering is achieved, it becomes possible to reduce noise by employing spectral subtraction [8]. Furthermore, by evaluating the noise power at each time and frequency, it is possible to assess the confidence level of discrimination results between healthy and defective sounds. Figure 2 illustrates the ego-noise and the average power spectrum values at different time points. Notably, inspections conducted during periods of minimal noise levels can be considered as high confidence inspections. Thus, by performing ego-noise prediction during hammering, it is possible to achieve noise reduction and assess the reliability of discrimination results between healthy and defective sounds. Based on the aforementioned considerations, ego-noise prediction during hammering holds significant potential for enhancing inspection discrimination accuracy. Consequently, this study aims to develop ego-noise prediction method for enhanced discrimination in UAV hammering inspection.

In the use of UAVs for hammering inspection, the sources of ego-noise are the exhaust system for cooling, propeller, and motor [9]. The sound emitted by the exhaust system maintains a steady pattern, enabling predictions based on the sound preceding the prediction. In contrast, the motor and propeller sounds exhibit variability, making them difficult to predict accurately. In this study, we aim to predict unsteady ego-noise by monitoring either the propeller or the motor, which are connected and operated as one unit.

Potential approaches to monitor the propeller or the motor involve utilizing the Rotations Per Minute (RPM) command, or RPM data obtained from the motor encoder. In practical scenarios, predicting the ego-noise generated by propellers presents challenges since the RPM command does not always precisely correspond to the actual motor operation. Consequently, it is difficult to accurately predict ego-noise in a real-world environment through RPM commands. Furthermore, commercial UAVs are often not equipped with encoders or do not have access to their RPM data obtained from the motor encoder. In this study, we do not use RPM data, instead we explore a simple and economical method for ego-noise prediction.

Another potential approach to monitor either the propeller or the motor involves capturing sound through a microphone installed on the propeller. To ensure that microphones do not inadvertently capture the target sound, proper isolation measures must be implemented. Wind pressure is extremely strong around the propellers of large drones, such as those used for hammering inspection, making propeller sound monitoring with microphones unsuitable [10].

Due to its resilience to external factors such as hammering sound and wind, we identified the vibration of the propeller as a suitable method for monitoring ego-noise sources in a simple and cost-effective manner. We propose an ego-noise prediction method by translating the modality of propeller vibrations into the modality of ego-noise sound, as shown in Fig. 3. For ease of measurement, we utilize propeller acceleration as a representation of propeller vibration.

B. Overview of ego-noise prediction

The overview of the proposed method is shown in Fig. 4. We assume that ego-noise is strongly related to the vibration frequencies of the propeller. Furthermore, the acceleration spectrogram represents the temporal evolution of the propeller's vibration frequencies. We utilize Recurrent Neural Network (RNN) [11] to predict the ego-noise spectrogram using the acceleration spectrogram as input. During the training phase, the RNN is trained using the Mean Absolute Error (MAE) between the actual and predicted ego-noise spectrograms. During the prediction phase, the acceleration representing propeller vibration is used as input, and the RNN predicts the ego-noise spectrogram.

First, time-synchronized ego-noise amplitude $e[m]$ and acceletion matrix $\boldsymbol{A}\,[n]$ with different sampling frequencies are obtained from the microphone and accelerometer installed on

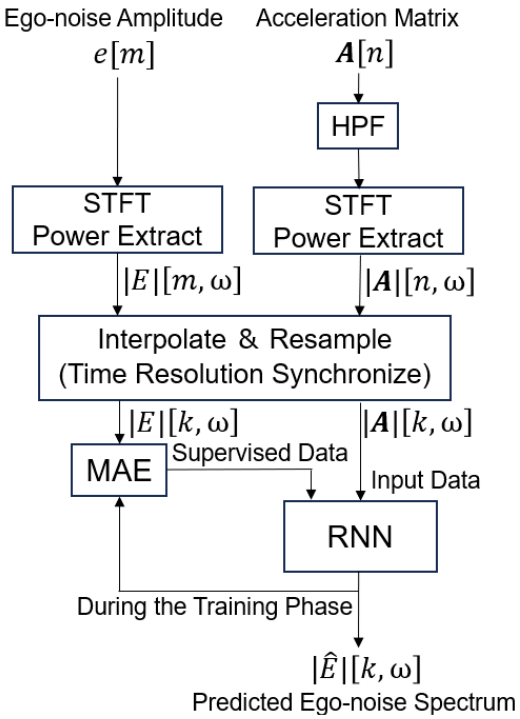

Fig. 4. Overview of ego-noise prediction. During the training phase, the RNN is trained using the MAE between the actual and predicted ego-noise spectrograms. During the prediction phase, the acceleration spectrogram representing propeller vibration is used as input, and the RNN predicts the ego-noise spectrogram.

the propeller.

$$\boldsymbol{A}[n] = \begin{bmatrix} a_{1\mathrm{x}}[n] & a_{1\mathrm{y}}[n] & a_{1\mathrm{z}}[n] \\ \vdots & \vdots & \vdots \\ a_{N\mathrm{x}}[n] & a_{N\mathrm{y}}[n] & a_{N\mathrm{z}}[n] \end{bmatrix}, \tag{1}$$

where $a_{N\mathrm{x}}[n]$ represents the acceleration of the Nth accelerometer along the x-axis at time n.

In the use of UAV for hammering inspection, hammering recoil, shaking due to wind, and the UAV's motions interfere with ego-noise prediction. A hammering machine known as the snap motor [12] is used for a hammering inspection robot [5]. The snap motor's hammer head and the body are connected by a flexible steel band. Thus, the hammering recoil is transmitted to the UAV only at low frequencies. The frequency of shaking due to wind and UAV's motion is less than 10 Hz [13]. By employing a high-pass filter to eliminate the low-frequency components, it becomes possible to predict ego-noise based on the acceleration data during hammering, as well as the pre-hammering period.

The ego-noise generated from the propellers is considered to be strongly related to its RPM. Additionally, it is assumed that the RPM has a strong relation with the vibration frequency of the propellers. To use this RPM-related information as a feature, Short Time Fourier Transform (STFT) is performed. To ensure that the time resolutions of the ego-noise and acceleration spectrograms match as closely as possible, we need to adjust the overlap rate of the STFT. The overlap rate refers to the amount of overlap between

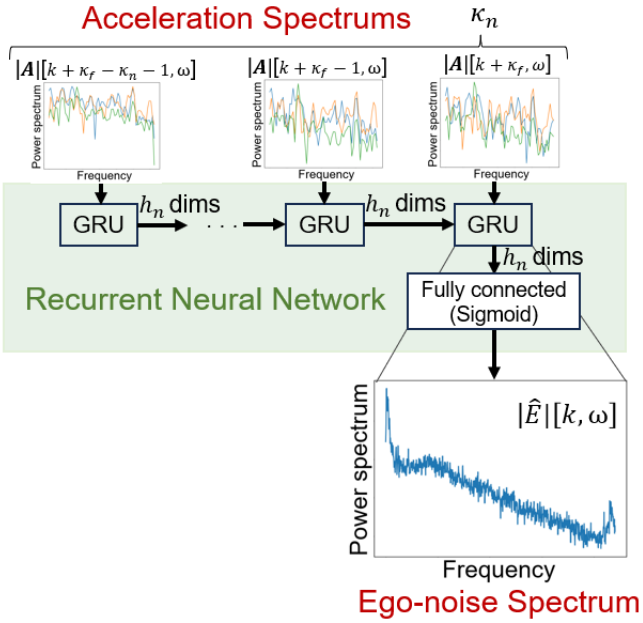

Fig. 5. RNN Predictor Architecture. κ_f is the number of acceleration spectra to be shifted, κ_n is the number of the acceleration spectra input to the RNN predictor, and h_n is the number of output dimensions of GRU.

consecutive time segments when computing the spectrogram. Interpolation and resampling are performed to perfectly match their time resolutions.

RNN has a recursive structure, making them particularly suitable for processing time-series data. RNN predicts the ego-noise spectrum by translating the acceleration spectra.

C. Architecture of RNN predictor

The specific architecture of RNN predictor is shown in Fig. 5. Variable κ_f is the number of acceleration frames to be shifted. Variable κ_n is the number of the acceleration spectrum input to the RNN predictor. Variable h_n is the number of output dimensions of Gated Recurrent Unit (GRU) [14].

Generally, GRU is used for tasks such as natural language processing and signal classification. However, in this study, we propose its use for memorizing the time-series features of acceleration spectra. GRU encodes the acceleration spectrum of κ_n along the time series. The number of output dimensions of the GRU is set to h_n to prevent overfitting by bottlenecking the middle part of the RNN predictor. Equation (2) shows the input-output mapping for a general fully connected neural network. The fully connected neural Network decodes to the ego-noise spectrum at time k from the h_n dimension variables compressed by time series encoding and bottlenecking with GRU.

$$y^j = f_{\mathrm{act}}\left(\sum_i w_i^j x_i^j + b^j\right), \tag{2}$$

where f_{act} is an activation function. The output value y^j of the jth neuron is obtained by passing the weighted sum of the input values x_i^j and the bias b^j through the activation function.

A Simple RNN is prone to gradient loss and is poor at memory retention because output recursion is multiplicative [15]. Equations (3)-(6) show latent state update steps in GRU.

$$\boldsymbol{R}_t = \sigma\left(W_R \boldsymbol{x}_t + U_R \boldsymbol{h}_{t-1} + b_R\right), \tag{3}$$

$$\boldsymbol{Z}_t = \sigma\left(W_Z \boldsymbol{x}_t + U_Z \boldsymbol{h}_{t-1} + b_Z\right), \tag{4}$$

$$\widetilde{\boldsymbol{h}}_t = \tanh\left\{W_h \boldsymbol{x}_t + U_h\left(\boldsymbol{R}_t \odot \boldsymbol{h}_{t-1}\right) + b_h\right\}, \tag{5}$$

$$\boldsymbol{h}_t = \left(1 - \boldsymbol{Z}_t\right) \odot \boldsymbol{h}_{t-1} + \boldsymbol{Z}_t \odot \widetilde{\boldsymbol{h}}_t, \tag{6}$$

where σ is the sigmoid function, $\odot$ is hadamard product (element-wise multiplication), $\boldsymbol{h}_t$ is output of hidden layer at time t, W is the weight matrix, and b is the bias term. $\boldsymbol{R}_t$ is the reset gate and controls how much of the old information is forgotten. $\boldsymbol{Z}_t$ is the update gate and controls the ratio of old information mixed with new information. Memory is updated through the Hadamard product of the previous hidden state $\boldsymbol{h}_{t-1}$ and the $\boldsymbol{R}_t$. This operation helps to retain important information and forget unnecessary elements from the previous memory state. Additionally, new information is incorporated using the weighted $\boldsymbol{x}_t$. In this way, $\widetilde{\boldsymbol{h}}_t$ is created with short-term memory. Finally, $\boldsymbol{h}_{t-1}$ and $\widetilde{\boldsymbol{h}}_t$ are mixed according to the ratio of $\boldsymbol{Z}_t$.

D. Evaluation of ego-noise prediction performance

To evaluate the accuracy of predictions, we utilize the Percentage Error (PE). PE$[k,\omega]$ represents the error rate at time k and angular frequency ω.

$$\mathrm{PE}\left[k,\omega\right] = 100\left(\frac{\left|\hat{E}\right|\left[k,\omega\right] - \left|E\right|\left[k,\omega\right]}{\left|E\right|\left[k,\omega\right]}\right), \tag{7}$$

where $\left|\hat{E}\right|\left[k,\omega\right]$ and $\left|E\right|\left[k,\omega\right]$ are the predicted and actual ego-noise spectra at time k angular frequency ω, respectively.

We compute Normalized Noise Prediction Error (NNPE) [16] to evaluate the overall prediction errors. NNPE computes the error of the ego-noise prediction normalized by the energy of the actual ego-noise, as follows:

$$\frac{1}{K}\sum_{k=1}^{K} 10\log_{10}\left(\frac{\sum_{\omega=1}^{\Omega}\left|\left|\hat{E}\right|\left[k,\omega\right]^2 - \left|E\right|\left[k,\omega\right]^2\right|}{\sum_{\omega=1}^{\Omega}\left|E\right|\left[k,\omega\right]^2}\right), \tag{8}$$

where K is number of time steps in the spectrogram, and Ω is number of angular frequency bins in the spectrogram. NNPE is a metric that calculates the difference between the predicted and actual energies of ego-noise for each angular frequency bin, normalized by the actual energy of ego-noise. Therefore, NNPE represents the ratio of the maximum residual ego-noise energy that may remain after ego-noise reduction through spectral subtraction to the ego-noise energy before ego-noise reduction.

III. EXPERIMENTS

A. Experimental equipment

The effectiveness of the proposed method was verified using data with varying ego-noise and propeller acceleration. A UAV (DJI M300 RTK) with a microphone (Audio-Technica AT875) and an accelerometer (SparkFun ADXL345) was mounted on a cargo stand, as shown in Fig. 6.

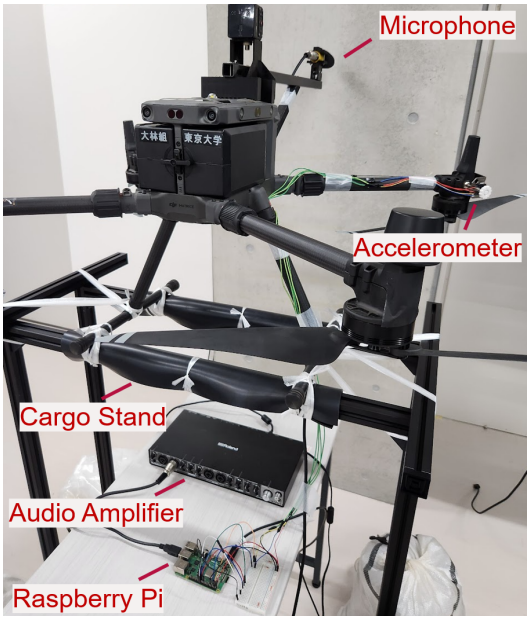

Fig. 6. Mounted UAV for ego-noise and acceleration measurement.

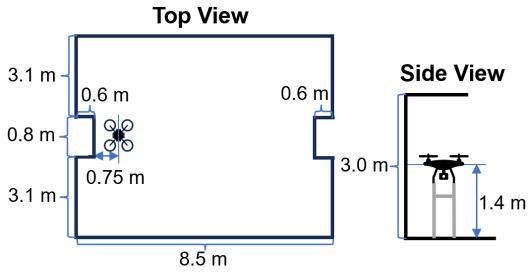

Fig. 7. Schematic of the experimental environment.

To verify the effectiveness of the proposed method against reverberating ego-noise, an experiment was conducted by placing the UAV indoors. The UAV was mounted facing a wall on a 1.4 m cargo stand, as shown in Fig. 7.

In a typical hammering inspection scenario, a single-directional microphone is used to effectively capture the hammering sound from the wall. Accordingly, this study uses a single-directional microphone to primarily capture the reverberating ego-noise. The microphone was placed at a distance of 6 cm from the wall. The sampling frequency of the microphone was 44.1 kHz.

In this study, all four propellers of the UAV were manually assigned the same time-varying rotational speed command by the UAV controller. Thus, only one accelerometer was sufficient for monitoring the propeller vibrations. The sampling frequency of the accelerometer was 2.5 kHz, and the measurement range was ±39.2 $\mathrm{m/s^2}$.

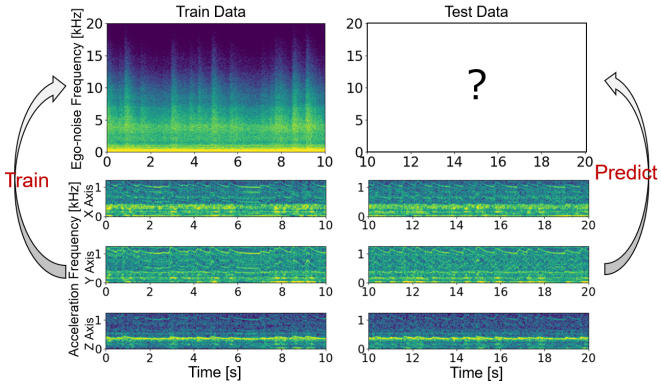

Fig. 8. Training and prediction overview. The first 10 s were used for training, and the last 10 s were used to test the prediction performance.

B. Processing parameters

Data was recorded for 20 s. The first 10 s were used for training, and the last 10 s were used to test the prediction performance, as shown in Fig. 8. The time resolution of both the acceleration and ego-noise spectrograms were synchronized at 25 ms. For this study, the training and testing spectrograms consisted of 400 samples since the duration of both the training and testing periods was set to 10 s.

The cutoff frequency of the acceleration high-pass filter was set to 20 Hz. The frequency resolution of the acceleration was 19.53 Hz and that of the ego-noise was 21.53 Hz. In this study, the ego-noise frequencies at which the predictions were performed were up to 20 kHz. The number of acceleration spectrum dimensions was 195 (65 dimensions $\times$ 3 axes) and the number of ego-noise spectrum dimensions was 950.

The RNN predictor was trained for 250 epochs and optimized with a MAE-based loss function and ADAM optimizer. Grid search was used to set κ_n to 15, κ_f to 2, and h_n to 95.

IV. RESULTS

Twelve datasets, where the timing, intensity, and rate of increase in propeller rotation speed varied, were evaluated using NNPE. The distribution of NNPE, with a median NNPE of -11.46 dB, is shown in Fig. 9. The predicted accuracy of ego-noise obtained through the proposed method was at a level that suggests the potential for effective ego-noise reduction, because NNPE represents the ratio of the maximum residual ego-noise energy that may remain after ego-noise reduction through spectral subtraction to the ego-noise energy before ego-noise reduction. Moreover, a study focused on template-based ego-noise prediction and demonstrated an improvement in the SNR from -3 dB to approximately 3 dB within the NNPE range of -12 to -6 situations [16].

Prediction errors due to blurring is shown in Fig. 10. Overpredictions and underpredictions are shown by shades of blue and red, respectively. When the spectrum power increases, there is a tendency of transition from underprediction

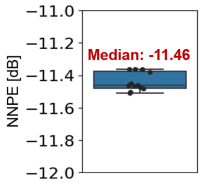

Fig. 9. NNPE for each of the 12 datasets.

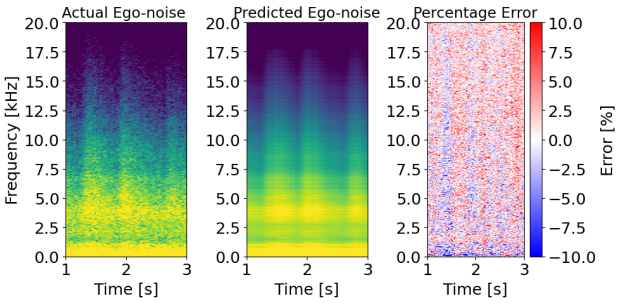

Fig. 10. Spectrograms of actual ego-noise (left), predicted ego-noise (middle), and PE (right).

to overprediction. This is primarily due to the fact that the predictions are blurred in the time direction. There are two types of blurring: time-directional blurring and frequency-directional blurring. Generally, there is a trade-off between stability and the ability to follow rapid changes, and a trade-off between model expressiveness and generalization performance. Time-directional blurring is considered to be a result of the acquisition of stability in the training phase, while the frequency-directional blurring is attributed to the bottleneck part of the RNN predictor. Moreover, we consider the blurring can be suppressed by improving the time and frequency resolution through increasing the sampling frequency of the accelerometer, and adjusting the overlap rate and window width of the STFT.

Figure 11(a) shows the actual ego-noise, and Fig. 11(b) shows our trained RNN successfully predicts the unsteady ego-noise spectrogram. A stripe-like pattern can be seen on the spectrogram. The power increases when the propeller rotates strongly and generates large ego-noise.

Figure 11(c) shows the predicted spectrogram of ego-noise for the initial training phase. In the early training phase, a steady spectrogram is predicted. The bias terms b^j (Eq. (2)) of the fully connected layers are learned first. By training the RNN just before prediction, such steady ego-noise can be predicted. This allows the prediction of both the steady ego-noise and the steady environmental noise.

V. DISCUSSION

In this study, we achieved the prediction of diverse and unsteady ego-noise of UAVs by implementing a framework that translates vibrations into ego-noise. This suggests that it enables the reduction of reverberating ego-noise, which cannot be achieved through space-filtering. We believe this study expanding the potential applications of acoustic sensing using UAVs.

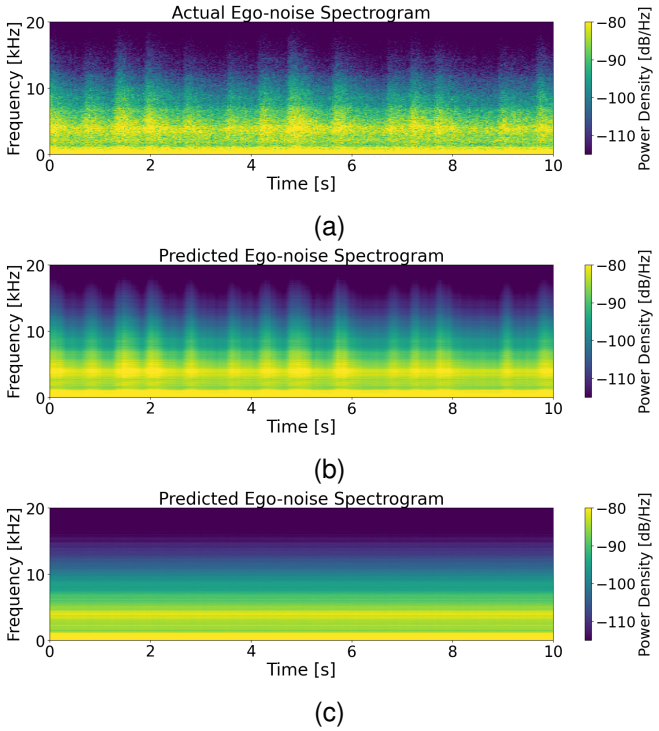

Fig. 11. Spectrograms of actual and predicted ego-noise: (a) actual ego-noise spectrogram, (b) predicted ego-noise spectrogram after 250 epochs of training, and (c) predicted ego-noise spectrogram in the initial training phase (after 3 epochs of training).

In this study, each of the four propellers of the UAV was manually given the same time-varying rotational speed command. Therefore, effective prediction was achievable with only 10 s of ego-noise and acceleration data for training. In reality, a longer duration of data is expected to be required for training due to the independent movement of the four propellers. Furthermore, there is a possibility of resonance when all four propellers are rotated simultaneously. It is essential to investigate to what extent this resonance occurs in real-flight scenarios and how it impacts the prediction of ego-noise.

VI. CONCLUSION

In this paper, we propose a novel ego-noise prediction framework by focusing on propellers as the main ego-noise source, and translating the modality of propeller vibrations into the modality of ego-noise sound. The prediction accuracy of ego-noise spectrograms was at a level that suggests the potential for effective ego-noise reduction. Therefore, the proposed method represents a significant step towards the effective reduction of reverberating ego-noise, and the results are promising for applications in UAV hammering inspection. As UAV technology advances and finds a wider range of applications, enhancing the auditory analysis on which UAVs rely becomes essential. Therefore, this research represents a crucial step towards ensuring clearer and more accurate sound sensing in UAV operations.

In the future works, we will verify that the proposed method actually improves the accuracy of hammering inspection based on the ego-noise reduction and the confidence evaluation of each discrimination result. Moreover, we will investigate ego-noise prediction techniques using RPM command, which do not necessitate the addition of extra sensors.

ACKNOWLEDGEMENT

This work was supported in part by JSPS KAKENHI under Grant Number JP21K17829.

REFERENCES

[1] J. Y. L. Kasahara, A. Yamashita, H. Asama, and H. Fujii, "Complementarity of sensors and weak supervision for defect detection in concrete structures," in *Proceedings of the 2020 IEEE/SICE International Symposium on System Integration (SII)*, 2020, pp. 1–6.

[2] J. Y. L. Kasahara, H. Fujii, A. Yamashita, and H. Asama, "Clustering of spatially relevant audio data using mel-frequency cepstrum for diagnosis of concrete structure by hammering test," in *Proceedings of the 2017 IEEE/SICE International Symposium on System Integration (SII)*, 2017, pp. 787–792.

[3] C. J. Salaan, K. Tadakuma, Y. Okada, K. Ohno, and S. Tadokoro, "UAV with two passive rotating hemispherical shells and horizontal rotor for hammering inspection of infrastructure," in *Proceedings of the 2017 IEEE/SICE International Symposium on System Integration (SII)*, 2017, pp. 769–774.

[4] L. Wang and A. Cavallaro, "Ear in the sky: Ego-noise reduction for auditory micro aerial vehicles," in *Proceedings of the 2016 13th IEEE International Conference on Advanced Video and Signal Based Surveillance (AVSS)*, 2016, pp. 152–158.

[5] Y. Nishimura, S. Takahashi, H. Mochiyama, and T. Yamaguchi, "Automated hammering inspection system with multi-copter type mobile robot for concrete structures," *IEEE Robotics and Automation Letters*, vol. 7, no. 4, pp. 9993–10 000, 2022.

[6] D. Mukhutdinov, A. Alex, A. Cavallaro, and L. Wang, "Deep learning models for single-channel speech enhancement on drones," *IEEE Access*, vol. 11, pp. 22 993–23 007, 2023.

[7] L. Wang and A. Cavallaro, "Acoustic sensing from a multi-rotor drone," *IEEE Sensors Journal*, vol. 18, no. 11, pp. 4570–4582, 2018.

[8] G. Ince, K. Nakadai, T. Rodemann, Y. Hasegawa, H. Tsujino, and J.-i. Imura, "Ego noise suppression of a robot using template subtraction," in *Proceedings of the 2009 IEEE/RSJ International Conference on Intelligent Robots and Systems*, 2009, pp. 199–204.

[9] D. Miljković, "Methods for attenuation of unmanned aerial vehicle noise," in *Proceedings of the 2018 41st International Convention on Information and Communication Technology, Electronics and Microelectronics (MIPRO)*, 2018, pp. 0914–0919.

[10] S. Yoon, S. Park, and S. Yoo, "Two-stage adaptive noise reduction system for broadcasting multicopters," in *Proceedings of the 2016 IEEE International Conference on Consumer Electronics (ICCE)*, 2016, pp. 219–222.

[11] I. Sutskever, O. Vinyals, and Q. V. Le, "Sequence to sequence learning with neural networks," in *Proceedings of the Advances in Neural Information Processing Systems*, vol. 27, 2014.

[12] K. Misu and H. Mochiyama, "Arched snap motor: power flow analysis," *Advanced Robotics*, vol. 35, no. 18, pp. 1107–1115, 2021.

[13] T. Chu, M. J. Starek, J. Berryhill, C. Quiroga, and M. Pashaei, "Simulation and characterization of wind impacts on suas flight performance for crash scene reconstruction," *Drones*, vol. 5, no. 3, p. 67, 2021.

[14] J. Chung, Ç. Gülçehre, K. Cho, and Y. Bengio, "Empirical evaluation of gated recurrent neural networks on sequence modeling," *Computing Research Repository*, vol. abs/1412.3555, 2014.

[15] M. Kaur and A. Mohta, "A review of deep learning with recurrent neural network," *International Conference on Smart Systems and Inventive Technology (ICSSIT)*, pp. 460–465, 2019.

[16] G. Ince, K. Nakadai, T. Rodemann, J.-i. Imura, K. Nakamura, and H. Nakajima, "Assessment of single-channel ego noise estimation methods," in *Proceedings of the 2011 IEEE/RSJ International Conference on Intelligent Robots and Systems*, 2011, pp. 106–111.